Theoretical analysis of multimagnon excitations in resonant inelastic x-ray scattering spectra of two-dimensional antiferromagnets

Subhajyoti Pal [1], Umesh Kumar [2], Prabhakar [1], and Anamitra Mukherjee [1,*]

[1] *School of Physical Sciences, National Institute of Science Education and Research, a CI of Homi Bhabha National Institute, Jatni 752050, India*

[2] *Department of Physics and Astronomy, Rutgers University, Piscataway, New Jersey 08854, USA*

(Received 10 May 2023; revised 11 November 2023; accepted 14 November 2023; published 5 December 2023)

Resonant inelastic x-ray spectroscopy (RIXS) has emerged as an important tool to explore magnetism in two-dimensional (2D) antiferromagnets realized in strongly correlated materials. Here, we consider the Heisenberg model with nearest- and next-nearest-neighbor hopping relevant to the study of magnetic excitations of the cuprate family. We compute the RIXS cross-section within the ultrashort core-hole lifetime expansion of the Kramers-Heisenberg scattering amplitude that allows a perturbative solution within linear spin wave theory (LSWT). We report detailed results for both spin-conserving and nonconserving channels. Apart from the widely discussed single-magnon and bimagnon contributions, we show that three-magnon contributions in the spin-nonconserving channel are useful to explain certain features of the RIXS data for 2D cuprates. We confirm the qualitative correctness of the LSWT conclusions for the three-magnon excitation with exact diagonalization. In this paper, we put constraints on the dispersion of the three-magnon in the Brillouin zone, opening avenues for realizing higher modes of quasiparticles using RIXS.

DOI: 10.1103/PhysRevB.108.214405

I. INTRODUCTION

Strongly correlated materials are known to host exotic quantum phenomena such as superconductivity, strange metallicity, confinement, and deconfinement. Two-dimensional (2D) cuprates are known to host a number of such properties and are one of the most studied materials in the condensed matter community [1,2]. More recently, superconductivity has also been discovered in the infinite layer (IL) nickelates, which is proposed as a cuprate analog [3]. Superconductivity in 2D iridates has also been proposed due to their similarity to cuprates but has yet to be realized [4]. The magnetism in these 2D materials is understood to play a central role in these exotic phenomena [5–7].

Resonant inelastic x-ray scattering (RIXS) has become an important tool in the recent past to explore magnetism in such strongly correlated materials [8,9]. The Kramers-Heisenberg (KH) formalism employed to simulate the RIXS cross-section is complex and makes interpreting RIXS data challenging [9–15]. Significant progress has been made in exploring quantum magnets using RIXS after the realization that it can allow for single spin-flip excitations at the L edge in cuprates [16–18] The ultrashort core-hole life (UCL) expansion of RIXS maps the cross-section to spin-conserving (SC) and nonspin-conserving (NSC) channels at the Cu L edge [13,19–22]. On the experimental side, progress has been made to resolve the polarization of the scattered RIXS spectra, therefore allowing for the filtering of spin-flip excitations [23,24]. Significant progress has been made in exploring the higher-order corrections in the SC channel RIXS, as this channel dominates the edge that does not allow for single spin flips [12,25,26]. However, there is limited work exploring the higher-order corrections in the NSC channel. The SC channel has been successful in identifying four-spinons in one-dimensional (1D) cuprates [12,26,27], multitriplons in a spin ladder [28–30], and multimagnons in 2D cuprates [31] in the phase space beyond traditional probes such as inelastic neutron scattering (INS), as this channel is usually inaccessible. On the other hand, the NSC channel of RIXS is usually understood to be equivalent to the INS probe, and the higher-order contributions have not been explored in the literature for the 2D cuprates. Recently, a number of experiments have reported multimagnons, attributing higher-order multimagnons in the RIXS cross-section [31,32].

Exploring the contributions of higher-order excitations has also greatly interested the INS community. For example, four-spinon contributions were reported in the INS response of 1D cuprates [33,34] and multitriplons in spin ladder cuprates [35,36]. The features beyond the conventional magnons were interpreted as fractionalized magnon excitations in 2D cuprates [37].

There has been a renewed interest in exploring the RIXS cross-section for the 2D cuprates [31,38–41]. Recently, RIXS has been used to characterize the influence of apical oxygen in different cuprates [39] by characterizing the features at higher energies at $(\pi, 0)$, using further nearest neighbors. The anomalous feature in 2D cuprates has been identified as fractional spin excitations [41]. In the past, some of the features in the inelastic neutron spectra have been attributed to fractionalized spin excitations arising from magnon-magnon interactions [37]. This leads to complications in

*anamitra@niser.ac.in

interpreting the additional features observed in RIXS experiments. Motivated by the recent identification of various correlation functions for the higher-order contributions in the UCL expansion of the KH formalism in 1D cuprates [19], we here explore these correlation functions in the context of 2D Heisenberg antiferromagnets (AFMs), realized in 2D cuprates [31] and IL nickelates [6].

In this paper, we report the distinct magnetic excitations realized in the SC and NSC channels of the UCL expansion of the RIXS cross-section employing standard linear spin-wave theory (LSWT) for 2D AFM Heisenberg Hamiltonian. We find the weakly dispersing multimagnon excitation reported for La_2CuO_4 in Ref. [31] can be qualitatively understood as originating from three-magnon excitation from our analysis. We further validate these conclusions with exact diagonalization (ED).

Our paper is organized as follows. In Sec. II, we introduce the spin model for the 2D Heisenberg AFMs explored in this paper and present the mapping of the spin Hamiltonian to magnons. We also introduce the response functions for the corrections in UCL expansion of the RIXS cross-section explored in this paper. In Sec. III, we present and discuss the results for the NSC and SC channels of RIXS cross-section evaluated using LSWT. We also compare the NSC channel LSWT results with ED for consistency. Finally, in Sec. IV, we conclude our findings and comment on the recent Cu L-edge data of 2D cuprates reported in the literature.

II. METHOD

The 2D AFMs realized in 2D cuprates consist of CuO_2 plaquettes. The corresponding one-band Hubbard model can be mapped to the spin-half Heisenberg model and can very well capture the low-energy spin dynamics realized in materials [11,42–44]. We, therefore, start with the 2D spin model on a square lattice given by

$$H_0 = J_1 \sum_{\langle ij \rangle} \mathbf{S}_i \cdot \mathbf{S}_j + J_2 \sum_{\langle\langle ij \rangle\rangle} \mathbf{S}_i \cdot \mathbf{S}_j. \tag{1}$$

Here, $\langle \cdots \rangle$ and $\langle\langle \cdots \rangle\rangle$ indicate the sum over nearest-neighbor (NN) and next-nearest-neighbors (NNN) sites, respectively. J_1 and J_2 are the superexchange couplings between NN and NNN sites. Also, $\mathbf{S}_i$ is the spin at site i. We assume the z axis as the quantization axis for the AFM and consider a bipartite lattice for the AFMs, with sublattices A and B. In this paper, we consider an AFM NN exchange. While the AFM NNN exchange is well established for the cuprate family from a theoretical standpoint, we also consider ferromagnetic (FM) NNN exchanges in this paper for completeness.

A. LSWT for H_0

We map the spin Hamiltonian to magnons using LSWT, using the usual notion of the bipartite lattice with sublattices A and B. In the AFM ground state, the Hamiltonian can be bosonized in LSWT, for which we introduce the standard Holstein-Primakoff (HP) transformation as follows:

$$\text{For sublattice A} = \begin{cases} \hat{S}_i^+ = \sqrt{2S}\sqrt{1 - \frac{a_i^\dagger a_i}{2S}}\, a_i \\ \hat{S}_i^- = \sqrt{2S} a_i^\dagger \sqrt{1 - \frac{a_i^\dagger a_i}{2S}} \\ \hat{S}_i^z = S - a_i^\dagger a_i. \end{cases} \tag{2}$$

$$\text{For sublattice B} = \begin{cases} \hat{S}_i^+ = \sqrt{2S} b_i^\dagger \sqrt{1 - \frac{b_i^\dagger b_i}{2S}} \\ \hat{S}_i^- = \sqrt{2S}\sqrt{1 - \frac{b_i^\dagger b_i}{2S}}\, b_i \\ \hat{S}_i^z = -S + b_i^\dagger b_i. \end{cases} \tag{3}$$

To diagonalize the Hamiltonian $\hat{H}_0$ in Eq. (1), we need to introduce the Bogoliubov transformation, which in reciprocal space is defined as

$$\begin{bmatrix} \alpha_{\mathbf{k}} \\ \beta_{-\mathbf{k}}^\dagger \end{bmatrix} = \begin{bmatrix} u_{\mathbf{k}} & v_{\mathbf{k}} \\ v_{-\mathbf{k}} & u_{-\mathbf{k}} \end{bmatrix} \begin{bmatrix} a_{\mathbf{k}} \\ b_{-\mathbf{k}}^\dagger \end{bmatrix}, \tag{4}$$

where

$$u_{\mathbf{k}} = \sqrt{\frac{1}{2} + \frac{\left(J_0^{AB} - J_0^{AA} + J_{\mathbf{k}}^{AA}\right)}{2\sqrt{\left(J_0^{AB} - J_0^{AA} + J_{\mathbf{k}}^{AA}\right)^2 - \left(J_{\mathbf{k}}^{AB}\right)^2}}},$$

$$v_{\mathbf{k}} = \text{sign}\left(J_{\mathbf{k}}^{AB}\right)\sqrt{u_{\mathbf{k}}^2 - \frac{1}{2}} \tag{5}$$

$$J_{\mathbf{k}}^{AB} = J_1[\cos(k_x a) + \cos(k_y a)],$$

$$J_{\mathbf{k}}^{AA} = J_{\mathbf{k}}^{AA} = 2J_2[\cos(k_x a)\cos(k_y a)]. \tag{6}$$

Here, a is the lattice constant. Hence,

$$\hat{H} = \sum_{\mathbf{k}} \epsilon_{\mathbf{k}}(\alpha_{\mathbf{k}}^\dagger \alpha_{\mathbf{k}} + \beta_{\mathbf{k}}^\dagger \beta_{\mathbf{k}}) + \text{const.}, \tag{7}$$

$$\epsilon_{\mathbf{k}} = 2S\sqrt{\left(J_0^{AB} - J_0^{AA} + J_{\mathbf{k}}^{AA}\right)^2 - \left(J_{\mathbf{k}}^{AB}\right)^2}. \tag{8}$$

In this paper, we use $S = \frac{1}{2}$, as 2D cuprates are known to host spin-$\frac{1}{2}$ in the 2D Heisenberg model.

B. RIXS intensity

The RIXS cross-section is given by the KH formalism; $I_{\text{RIXS}} = \sum_f |\langle f|D_{\text{out}} O D_{\text{in}}|g\rangle|^2 \delta(E_f - E_g - \omega)$. Here, $|g\rangle(|f\rangle)$ are the ground (final) states from the Hamiltonian H_0 with energy $E_g\,(E_f)$, and ω is the energy loss. Also, $D_{\text{in(out)}}$ is the dipole operator, and O accounts for the evolution of the system given in the presence of the core hole. We refer to recent literature for a detailed exposition of the simplification of the cross-section (see Ref. [19]). Following the literature [19,20], we employ UCL approximation. This introduces a broadening factor (Γ), which is the inverse of the core-hole lifetime. In Appendix A, we outline that a perturbation in (J/Γ) leads to two distinct contributions to the RIXS intensity, namely, the NSC ($\Delta S = 1$) and SC ($\Delta S = 0$) channels. In what follows, we set $\hbar = 1$. The RIXS intensity $I_{\text{RIXS}} \propto \sum_l S_l^{\text{NSC}}(\mathbf{q}, \omega) + \sum_l S_l^{\text{SC}}(\mathbf{q}, \omega)$. Here, $\mathbf{q}(= \mathbf{k}_{\text{out}} - \mathbf{k}_{\text{in}})$ is the momentum transfer to the lattice. The proportionality constant involves polarization-dependent matrix elements arising out of the dipole operators which are different for the NSC and SC channels (see Ref. [16]). In Appendix A, we provide the SC

and NSC UCL expansions based on the contributions to the RIXS intensity. We explore both channels using the following response functions in this paper.

1. NSC channel

The RIXS intensity can be decomposed into a sum of terms of $O(\frac{1}{\Gamma^{2l}})$ with the lth-order contribution to the intensity given by

$$S_l^{\rm NSC}(\mathbf{q},\omega) = \frac{1}{\Gamma^{2l+2}} \sum_f \left| \langle f | \frac{1}{\sqrt{N}} \sum_i \exp(i\mathbf{q}\cdot\mathbf{R}_i) O_{i,l}^{\rm NSC} |g\rangle \right|^2 \times \delta(E_f - E_g - \omega),$$

where N is the total number of lattice sites. From Eq. (A1), we have (i) $O_{i,0}^{\rm NSC} = S_i^x$ for $l = 0$; (ii) $O_{i,1}^{\rm NSC} = \sum_{j\in \text{NN +NNN of } i} J_{i,j} S_i^x \mathbf{S}_i \cdot \mathbf{S}_j$, where i is the location where the core-hole is created; and (iii) $O_{i,2}^{\rm NSC} = \sum_{j\neq k; j,k\in \text{NN of } i} J_{i,j} J_{i,k} S_i^x \mathbf{S}_j \cdot \mathbf{S}_k$ for $l = 2$. We pictorially represent the summed-over bonds around i considered in $O_{i,1}^{\rm NSC}$ and $O_{i,2}^{\rm NSC}$ later in the paper.

2. SC channel

The lth-order contribution to the RIXS intensity in the SC channel is

$$S_l^{\rm SC}(\mathbf{q},\omega) = \frac{1}{\Gamma^{2l+2}} \sum_f \left| \langle f | \frac{1}{\sqrt{N}} \sum_i \exp(i\mathbf{q}\cdot\mathbf{R}_i) O_{i,l}^{\rm SC} |g\rangle \right|^2 \times \delta(E_f - E_g - \omega),$$

From Eq. (A2), we have (i) $O_{i,0}^{\rm SC} = n_i$, (ii) $O_{i,1}^{\rm SC} = \sum_{j\in \text{NN +NNN of } i} J_{i,j} \mathbf{S}_i \cdot \mathbf{S}_j$, and (iii) $O_{i,2}^{\rm SC} = \sum_{j\neq k; j,k\in \text{NN of } i} J_{i,j} J_{i,k} (\mathbf{S}_i \cdot \mathbf{S}_j)(\mathbf{S}_i \cdot \mathbf{S}_k)$, as above. Notice that the $l = 0$ order term does not lead to magnetic excitations and contributes to only the elastic scattering in the RIXS cross-section.

III. RESULTS AND DISCUSSIONS

We investigate the spin Hamiltonian given by Eq. (1) and limit ourselves to the LSWT approach. Within the UCL approximation of the KH formalism, the RIXS spectra can be mapped to a set of correlation functions in the SC and NSC channels, as presented above. We here report the responses until the second-order corrections of the UCL approximation. In this paper, we set the work in the regime $|J_2| < J_1$. We consider positive (negative) J_2 suppressing (promoting) the overall $J_2 = 0$ AFM order.

We present the Brillouin zone and momentum path for the 2D lattice in Fig. 1(a) explored for the ease of the readers. We plot our results in $\Gamma(0,0) - X(\pi,0) - M(\pi,\pi) - \Gamma(0,0)$ as highlighted in the figure unless otherwise stated.

As there is limited discussion on the higher-order corrections in the NSC channel, we start by presenting our results in this channel. Later, we report the results in the relative SC channel, extending it with long-range interactions in the correlation functions.

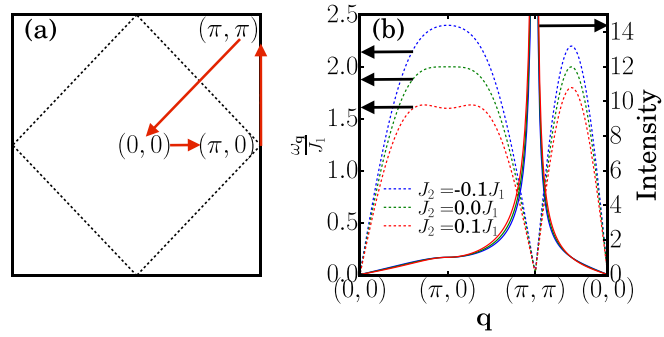

FIG. 1. Dashed lines in (a) show the magnetic Brillouin zone boundary. (b) Magnon dispersion (dashed line) and the momentum dependence of one magnon integrated resonant inelastic x-ray spectroscopy (RIXS) intensity (solid lines) for the two-dimensional (2D) extended Heisenberg model. The momentum is taken along the arrows, shown in (a).

A. NSC channel

In this section, we present results until the second-order correction in the UCL approximations. One peculiar feature of this channel is that there are an odd number of spin flips due to additional spin-flip mediated by the core-hole orbital with large spin-orbit coupling. Therefore, this channel is usually forbidden at the K edge.

1. Zeroth order

At the zeroth order in the UCL expansion, the NSC channel allows for a single spin-flip mediated by the core-hole orbital. The scattering operator is, therefore, given by

$$O_{\mathbf{q},0}^{\rm NSC} = \sum_i \exp(i\mathbf{q}\cdot\mathbf{r}_i) S_i^x. \tag{9}$$

We have preferentially chosen the spin-flip along the plane (along the x direction, here). We must do this, as the bipartite lattice used for the evaluating ground state fixes a quantization axis. If we can write the ground state without this, then one can consider either component of the operator for spin [19]. Using the LSWT approach discussed above, the operator can be mapped to the AFM magnon basis and is given by

$$O_{\mathbf{q},0}^{\rm NSC} \approx \sqrt{\frac{2SN}{2}} (u_\mathbf{q} - v_\mathbf{q})(\alpha_\mathbf{q} + \beta_\mathbf{q} + \alpha_{-\mathbf{q}}^\dagger + \beta_{-\mathbf{q}}^\dagger). \tag{10}$$

Notice that the operator can create a magnon in the vacuum, leading to a single-magnon scattering.

Figure 1(b) shows the zeroth-order response for a 2D AFM lattice with NNN couplings. This is also equivalent to the dynamical spin structure factor $S(q,\omega)$ observed in INS. We plot the magnon dispersion, evaluated using LSWT and the integrated intensity for the $S(q,\omega)$ response. We notice hardening of magnon dispersion for negative J_2, prominently at $(\pi,0)$ and $(\pi/2,\pi/2)$. The hardening at $(\pi,0)$ is relatively larger than $(\pi/2,\pi/2)$. Conversely, there is softening for positive J_2. The signatures of these are also seen in the sharpening of the intensity around (π,π) for $J_2 < 0$ compared with $J_2 = 0$. Our negative J_2 results are consistent with the literature [16]. Also, positive J_2 results clearly weaken the AFM order. Such studies by varying the relative magnitude of J_2/J_1 have been

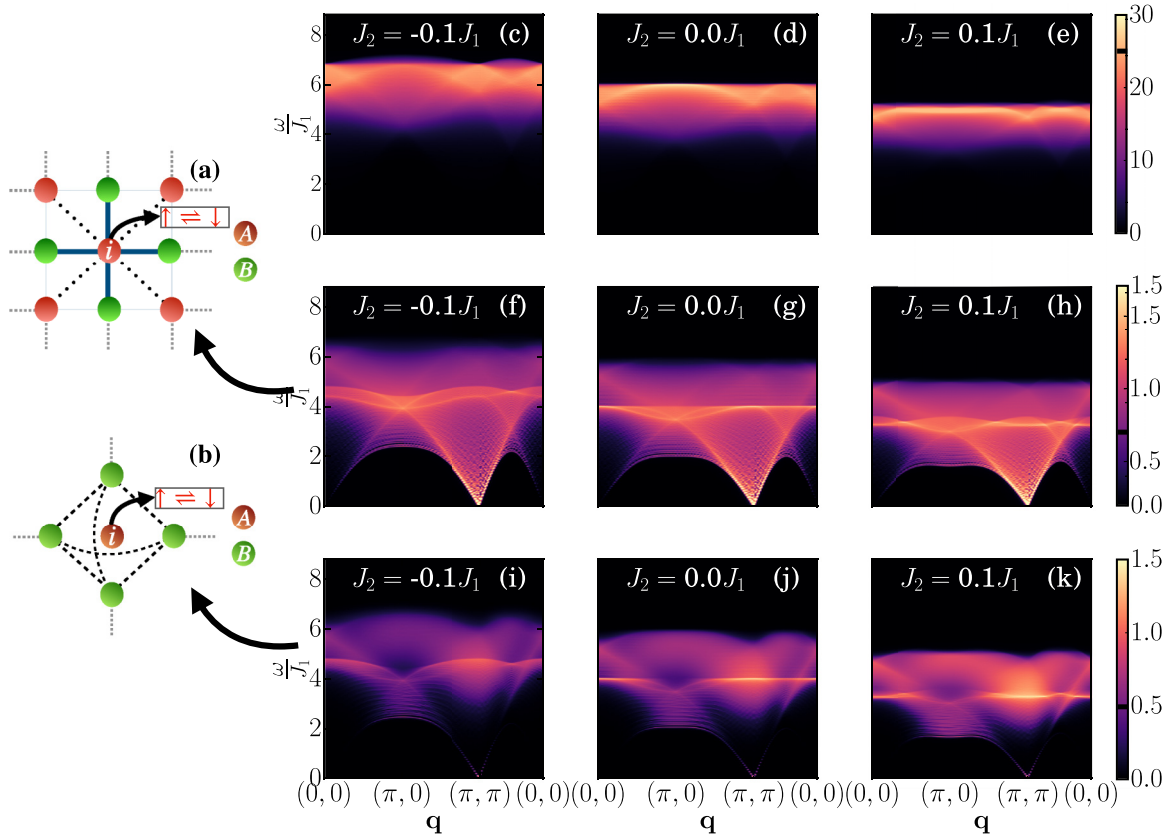

FIG. 2. Resonant inelastic x-ray spectroscopy (RIXS) spectra in the nonspin-conserving (NSC) channel. Schematic of contributions of (a) first-order and (b) second-order terms to the RIXS spectra, in the NSC channels corresponding to Eqs. (11) and (16). Three-magnon density of states (DOS) for the extended Heisenberg antiferromagnet for (c) $J_2 = -0.1J_1$, (d) $J_2 = 0$, and (e) $J_2 = 0.1J_1$. First-order correction of spectra for (f) $J_2 = -0.1J_1$, (g) $J_2 = 0$, and (h) $J_2 = 0.1J_1$. Second-order correction of RIXS spectra for (i) $J_2 = -0.1J_1$, (j) $J_2 = 0$, and (k) $J_2 = 0.1J_1$. To faithfully reproduce the data in the colormaps, we use a piecewise function with a boundary U_0, marked in black in the color bars of the respective plots. Below U_0, a linear map is used to represent the data. Above U_0, a logarithmic scale is used $U = U_0 + \ln_{10}[f(\mathbf{q}, \omega)] - \ln_{10}(U_0)$. Here, $f(\mathbf{q}, \omega)$ denotes the $(\mathbf{q}, \omega)$-dependent three-magnon DOS in (c) to (e) and RIXS spectra in (f) to (k).

used to explain certain aspects of the RIXS features of 2D cuprates [39] in the recent past.

B. NSC channel: Higher orders

As mentioned earlier, the NSC channel involves an odd number of spin flips. The higher-order correction can be described as a product of the single and double spin-flip operators. In principle, single and bimagnon excitations can be created both independently as well as combined. Figures 2(a) and 2(b) depict the first- and second-order NSC excitations, as discussed below. Since these excitations depend on the three-magnon density of states (DOS), we first discuss them.

The three-magnon DOS $A_{3M}(\omega)$, is given by the convolution of three one-magnon DOSs and is given by $A_{3M}(\omega) = \sum_{\omega',\omega''} A_{1M}(\omega - \omega' - \omega'')A_{1M}(\omega')A_{1M}(\omega'')$. Here, $A_{1M}(\omega) = \sum_{\mathbf{k}} \delta(\omega - \epsilon_{\mathbf{k}})$, and the dispersion $\epsilon_{\mathbf{k}}$ is given in Eq. (8). The three-magnon DOSs are shown in Figs. 2(c)–2(e). They result from the convolution of three one-magnon DOSs for $J_2 = -0.1$, 0.0, and 0.1, respectively. We notice hardening in both the energy of the DOS as well as spectral weight of the three-magnon for negative J_2 but softening for positive J_2. In addition, we observe that the three-magnon DOS shows weak $\mathbf{q}$ dependence compared with the other cases discussed above.

1. First order

The first-order correction in the UCL expansion of the NSC channel leads to correction with a prefactor at $O(J^2/\Gamma^4)$ (where J is the typical magnetic-exchange J_1), as shown in Eq. (A1). The scattering operator is given by

$$O^{\mathrm{NSC}}_{\mathbf{q},1} = \sum_{i,j} \exp(i\mathbf{q}\cdot\mathbf{r}i) J_{i,j} S^x_i (\mathbf{S}_i \cdot \mathbf{S}_j). \tag{11}$$

Here, the sum over i, j runs over the NN and NNN sites, as in the Hamiltonian H_0. Notice that the operator involves a single spin flip along with double spin flips. The schematic is shown in Fig. 2(a). Solid and dotted lines represent the NN and NNN terms, respectively. Keeping only the linear terms in LSWT, the operator (at A) can be mapped to bipartite bosons as

$$S^x_i \mathbf{S}_i \cdot \mathbf{S}_j \approx \sqrt{2S}(a^\dagger_i + a_i) \times [-S^2 + S(a_i b_j + a^\dagger_i b^\dagger_j + a^\dagger_i a_i + b^\dagger_j b_j)]. \tag{12}$$

We can rewrite the operator as $O^{\rm NSC}_{\mathbf{q},1} = O^{\rm NSC}_{\mathbf{q},1'} + O^{\rm NSC}_{\mathbf{q},1''}$. The first term $O^{\rm NSC}_{\mathbf{q},1'}$ consists of only a single bosonic operator and can be mapped to a single magnon operator. The second term $O^{\rm NSC}_{\mathbf{q},1''}$ consists of three bosonic operators and can be mapped to three-magnons which are given by

$$O^{\rm NSC}_{\mathbf{q},1''} = \frac{S^{3/2}}{\sqrt{2N}} \sum_{\mathbf{k},\mathbf{p}} [f_0(\mathbf{k},\mathbf{p},\mathbf{q})\alpha^\dagger_{-\mathbf{p}}\beta^\dagger_{-\mathbf{k}}\alpha^\dagger_{\mathbf{k}+\mathbf{p}+\mathbf{q}} + f_1(\mathbf{k},\mathbf{p},\mathbf{q})\beta^\dagger_{-\mathbf{p}}\beta^\dagger_{-\mathbf{k}}\alpha^\dagger_{\mathbf{k}+\mathbf{p}+\mathbf{q}}]. \quad (13)$$

The detailed expressions for $f_0(\mathbf{k},\mathbf{p},\mathbf{q})$ and $f_1(\mathbf{k},\mathbf{p},\mathbf{q})$ terms are presented in Appendix B.

Figures 2(f)–2(h) show the response for the first-order correction given from the first-order corrections for $J_2 = -0.1J_1, J_1$, and $0.1J_1$, respectively. This has a weak one-magnon feature and a three-magnon. The three-magnon ($J_2 = 0$) has three primary features: (i) a dispersing band up to $4J_1$ with a spread of $4J_1$, (ii) a band localized at $4J_1$, and (iii) a band that appears to disperse up to $5J_1$. Panels (f) and (h) show the results of finite J_2 and highlight that these features are pushed to higher and lower energy for $J_2 < 0$ and $J_2 > 0$, akin to the single-magnon case discussed previously.

2. Second Order

The second-order correction consists of a single spin flip along with a square of the double spin flips and contributes at $\sim O(J^4/\Gamma^6)$. The scattering operator is given by

$$O^{\rm NSC}_{\mathbf{q},2} = \sum_{\langle i,j,k\rangle} \exp(i\mathbf{q}\cdot\mathbf{r}i) J_{ij}J_{ik}S^x_i(\mathbf{S}_i\cdot\mathbf{S}_j)(\mathbf{S}_i\cdot\mathbf{S}_k). \quad (14)$$

The double spin-flip part can be rewritten as [19,25]

$$J_{i,j}J_{i,k}(\mathbf{S}_i\cdot\mathbf{S}_j)(\mathbf{S}_i\cdot\mathbf{S}_k) \approx -\tfrac{1}{2}J^2_{i,j}(\mathbf{S}_i\cdot\mathbf{S}_j) + \tfrac{1}{4}J_{i,j}J_{i,k}(\mathbf{S}_j\cdot\mathbf{S}_k). \quad (15)$$

The four-spin can effectively be mapped to two two-spins, with NN interactions and longer-range interactions. The first term has the spin-operator indices as i, j run over the NN. Since this term has the same form as that in the operator in the first order except for a different prefactor, it gives rise to no new features. We thus focus only on the second term of Eq. (15). The second term in the expression consists of long-range double spin flips, j and k indices, which are NN of the core-hole site i. The schematic for this is shown in Fig. 2(b).

The new correlation in this order, therefore, is given by

$$O^{\rm NSC}_{\mathbf{q},2'} = \sum_{i,j,k} \exp(i\mathbf{q}\cdot\mathbf{r}_i) J_{i,j}J_{i,k}S^x_i(\mathbf{S}_\mathbf{j}\cdot\mathbf{S}_k). \quad (16)$$

As discussed for the first order, the HP transformation for this also yields two terms:

$$S^x_i\mathbf{S}_j\cdot\mathbf{S}_k \approx \sqrt{2S}(a^\dagger_i + a_i) \times[-S^2 + S(a_jb_k + a^\dagger_jb^\dagger_k + a^\dagger_ja_j + b^\dagger_kb_k)]. \quad (17)$$

Again, the operator can be rewritten as $O^{\rm NSC}_{\mathbf{q},2'} = O^{\rm NSC,1}_{\mathbf{q},2'} + O^{\rm NSC,2}_{\mathbf{q},2'}$. The first term $O^{\rm NSC,1}_{\mathbf{q},2'}$ turns out to contribute to only single spin-flip excitations akin to the zeroth order. The second term has a distinct form and can contribute to multi-particle excitations. After the Bogoliubov transformation, the second term is given by

$$O^{\rm NSC,2}_{\mathbf{q},2'} \approx \frac{S^{3/2}}{\sqrt{2N}} \sum_{\mathbf{k},\mathbf{p}} f(\mathbf{k},\mathbf{p},\mathbf{q})[(v_\mathbf{p}u_{\mathbf{k}+\mathbf{q}-\mathbf{p}}v_\mathbf{k} - u_\mathbf{p}v_{\mathbf{k}+\mathbf{q}-\mathbf{p}}u_\mathbf{k})\alpha^\dagger_\mathbf{p}\alpha^\dagger_{\mathbf{k}+\mathbf{q}-\mathbf{p}}\beta^\dagger_{-\mathbf{k}} + (v_\mathbf{p}v_{\mathbf{k}+\mathbf{q}-\mathbf{p}}u_\mathbf{k} - u_\mathbf{p}u_{\mathbf{k}+\mathbf{q}-\mathbf{p}}v_\mathbf{k})\beta^\dagger_\mathbf{p}\alpha^\dagger_{\mathbf{k}+\mathbf{q}-\mathbf{p}}\beta^\dagger_{-\mathbf{k}}], \quad (18)$$

where $f(\mathbf{k},\mathbf{p},\mathbf{q}) = (J_1)^2[-6\{\cos(q_x - p_x) + \cos(q_y - p_y)\} + 2\{\cos(2k_x + q_x - p_x) + \cos(2k_y + q_y - p_y)\} + 4\{\cos(k_y)\cos(k_x + q_x - p_x) + \cos(k_x)\cos(k_y + q_y - p_y)\}]$.

We have, therefore, mapped this order to three-magnon excitations in the AFM lattice akin to the first order but with a distinct form.

Figures 2(i)–2(k) show the corresponding three-magnon response function for Eq. (16). The three-magnon spectral weight has a clear feature peak around $\omega = 4J_1$ and at $\mathbf{q} = 0$ for $J_2 = 0$ that remains finite for all q values in the Brillouin zone. The signature of one-magnon excitation is clearly seen in the sharp band in (i) dispersing through the Brillouin zone whose energy spread agrees with the single-magnon spectrum in Fig. 1(b). The intensity is, however, strongly suppressed. This feature has no contribution at $q = 0$ due to vanishing one-magnon DOS. Similar features are also seen in Figs. 2(j) and 2(k). The continuumlike feature in (i)–(k) with finite spread across the full Brillouin zone arises from $O^2_\mathbf{q}$, which does not commute with H_0 at any q.

Like the first-order case, the responses with finite J_2 shown in panels (i) and (k) reveal softening (hardening) for $J_2 > 0$ ($J_2 < 0$). However, the intensity is stronger for $J_2 > 0$ and weakened for $J_2 < 0$. The latter is true because, for $J_2 < 0$, the AFM order is strengthened, and thus, spin-flip excitation arising from the AFM is more dominant than for $J_2 < 0$. We conclude the LSWT discussion on the NSC channel by presenting in Fig. 3(a) the consolidated contributions from the NSC channel up to second order of the RIXS intensity. For this plot, we set Γ/J_1 to 5 [25]. We observe that, relative to the one-magnon contribution, the higher-order contributions are significant.

C. NSC channel: ED

We have also checked the consistency of the LSWT results against small-cluster ED. In Figs. 3(b) and 3(c), we show the three-magnon susceptibility on a 4×4 lattice at first and second order, respectively. In (b), we clearly see a small peak at $[\mathbf{q} = (0,0)]$ that disperses across the full Brillouin zone, as we have concluded from the LSWT. We also see a clear energy gap between the low-energy excitation, lying between $\omega = 0$ to $\sim 2J_1$, and the higher-energy excitations $>4J_1$. Similarly, in (c), we observe that the low-energy excitations are slightly pushed down $<2J_1$ but separated from the higher-

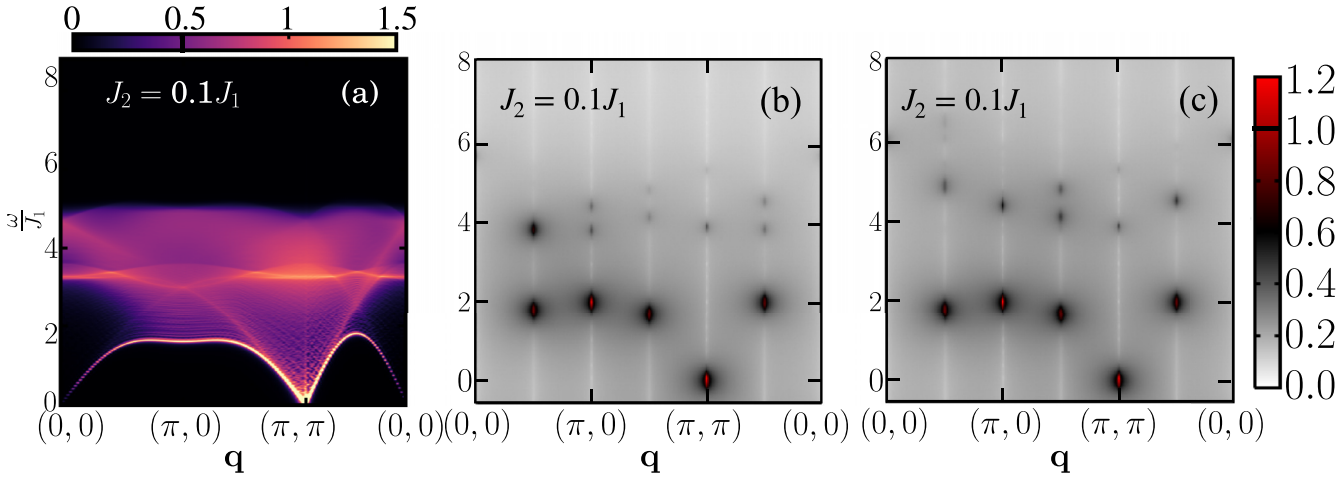

FIG. 3. Comparison of linear spin-wave theory (LSWT) with the small cluster (4×4 lattice) exact diagonalization (ED) results in the nonspin-conserving (NSC) channel. (a) Total contribution to the NSC channel up to the second order in the ultrashort core-hole lifetime (UCL) expansion evaluated using LSWT. Here, Γ is set equal to $5J_1$. ED results of the (b) first-order and (c) second-order contributions, for $J_2 = 0.1J_1$, corresponding to Eqs. (11) and (16), respectively. The vertical lines in (b) and (c) denote the allowed values of momentum transfer. The colormaps are generated using the same scheme as discussed in Fig. 2. The boundary value U_0 is indicated in black in the respective color bars.

energy excitations. By examining the basis-state contributions to the various peaks over the Brillouin zone, we find that the features below $\omega/J_1 = 2$ are primarily made out of one-flip basis states. This strongly suggests that the low-energy LSWT spectra are indeed generated by single-magnon excitations. Similarly, the high-energy features are made up of multiple spin-flip basis states. However, due to severe size limitations, the excitation energies are quite high, so the ED results simply provide a qualitative check of the contributions in the NSC channel. Thus, the broad takeaway from the ED results is that the NSC channel produces high-energy excitation that has finite spectral weight over the entire Brillouin zone.

D. SC channel

Here, we discuss the contributions from the SC channel of the UCL approximation of the KH formalism. This channel has been discussed in the context of SC edges in RIXS. For example, a two-magnon at the oxygen K-edge RIXS of a cuprate was reported [45]. With the improved RIXS resolution, the SC channel can also be realized at the Cu L edge and has been explored in 1D chains [13,19]. Therefore, we revisit this channel in the context of the L edge and provide results for $J_2 \neq 0$ for a 2D lattice. The computed three-magnon excitations overlap with two-magnon DOS; these results help us rule out whether these NNN terms can contribute to the new phase allowed in the NSC channel.

1. Zeroth order

The SC channel does not allow any spin flip at the zeroth order. Therefore, magnetic excitation is forbidden, and it contributes only to elastic scattering for the spin model.

E. SC channel: Higher orders

The higher-order corrections in the SC channel is given by an even number of multiple spin flips and can lead to magnetic excitations. Here, we investigate the dynamical correlation functions relevant to the two-magnon excitations in this channel. In this channel, for completeness, we also explore the correlation function with the NNN. This will further highlight why one needs the NSC channel to reproduce the features in the RIXS spectra of 2D AFMS.

The leading corrections in this channel map to the two-magnon. The two-magnon DOS $A_{2M}(\omega)$ is given by the convolution of two one-magnon DOSs, $A_{2M}(\omega) = \sum_{\omega'} A_{1M}(\omega - \omega')A_{1M}(\omega')$, with $A_{1M}(\omega) = \sum_{\mathbf{k}} \delta(\omega - \epsilon_{\mathbf{k}})$, see Eq. (8) We show the two-magnon DOS for $J_2 = -0.1, 0$ and 0.1 in Figs. 4(c)–4(e).

1. First order

The first-order correction in the UCL expansion of $O(J^2/\Gamma^4)$ is given by double spin flips. The scattering operator for this is given by

$$O^{\mathrm{SC}}_{\mathbf{q},1} = \sum_{i,j} \exp(i\mathbf{q}\cdot\mathbf{r}_i) J_{i,j} \mathbf{S}_i \cdot \mathbf{S}_j. \tag{19}$$

Here, the sum over i, j runs over the NN and NNN sites as in the Hamiltonian H_0. These NN (solid) and NNN (dashed) bonds are shown in Fig. 4(a).

With the HP transformation, Eq. (19) can be expressed as

$$O^{\mathrm{SC}}_{\mathbf{q},1} \approx S \sum_{\mathbf{k}\in BZ} [f_0(\mathbf{k},\mathbf{q})(a^\dagger_{\mathbf{k}-\mathbf{q}/2} a_{\mathbf{k}+\mathbf{q}/2} + b^\dagger_{\mathbf{k}-\mathbf{q}/2} b_{\mathbf{k}+\mathbf{q}/2}) + f_1(\mathbf{k},\mathbf{q})(a_{\mathbf{k}-\mathbf{q}/2} b_{-\mathbf{k}-\mathbf{q}/2} + a^\dagger_{\mathbf{k}+\mathbf{q}/2} b^\dagger_{-\mathbf{k}-\mathbf{q}/2})]. \tag{20}$$

Finally, the Bogoliubov transformation yields Eq. (19) in the form:

$$O^{\mathrm{SC}}_{\mathbf{q},1} \approx S \sum_{\mathbf{k}\in BZ} [-f_0(\mathbf{k},\mathbf{q})(u_{\mathbf{k}+\mathbf{q}/2} v_{\mathbf{k}-\mathbf{q}/2} + u_{\mathbf{k}-\mathbf{q}/2} v_{\mathbf{k}+\mathbf{q}/2}) + f_1(\mathbf{k},\mathbf{q})\big(u_{\mathbf{k}+\mathbf{q}/2} u_{\mathbf{k}-\mathbf{q}/2} + v_{\mathbf{k}+\mathbf{q}/2} v^\dagger_{\mathbf{k}-\mathbf{q}/2}\big)] \times (\alpha_{\mathbf{k}+\mathbf{q}/2}\beta_{-\mathbf{k}+\mathbf{q}/2} + \alpha^\dagger_{\mathbf{k}-\mathbf{q}/2}\beta^\dagger_{-\mathbf{k}-\mathbf{q}/2}), \tag{21}$$

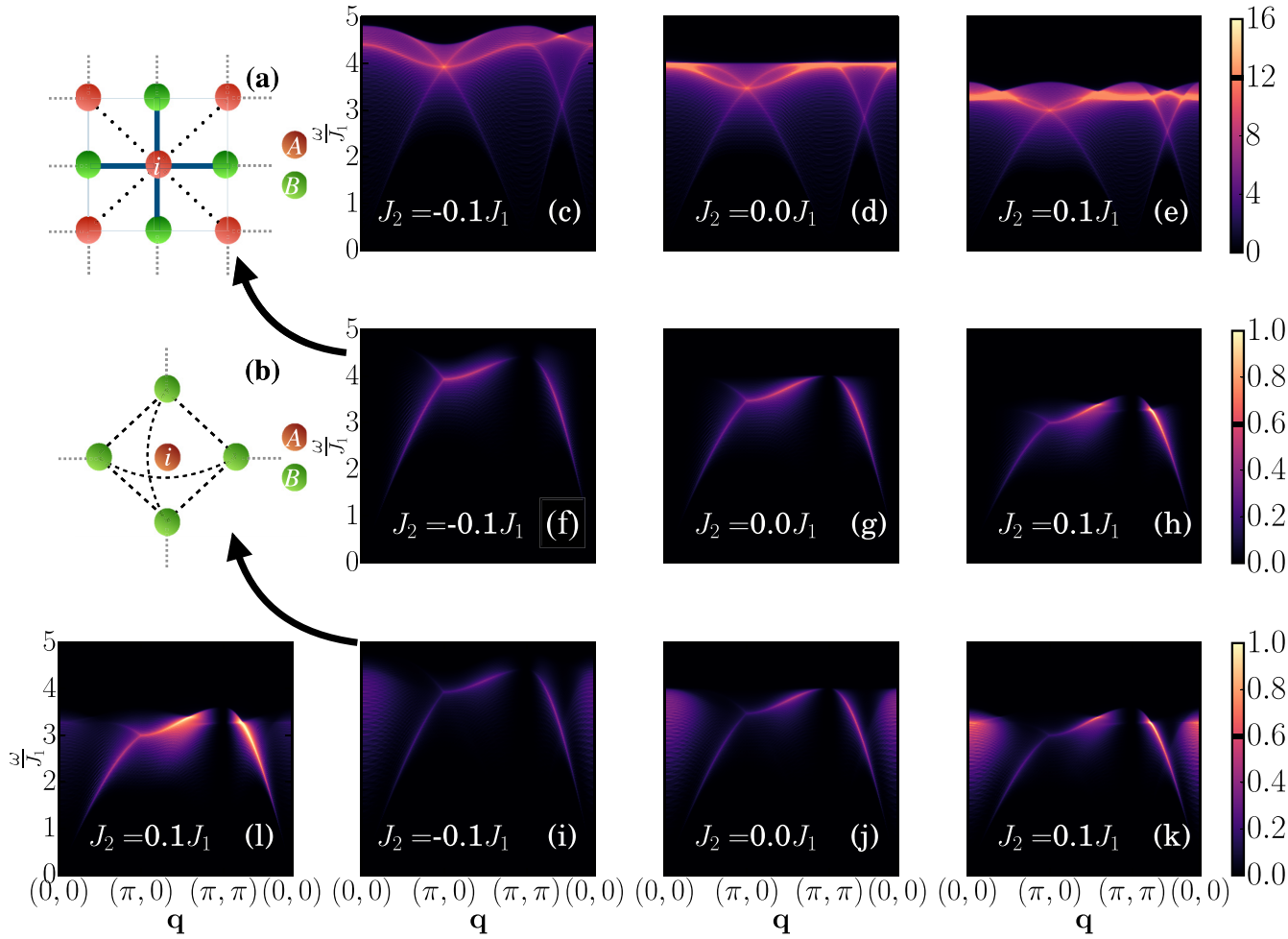

FIG. 4. Resonant inelastic x-ray spectroscopy (RIXS) spectra in the spin-conserving (SC) channel. Schematic of contributions of (a) first-order and (b) second-order terms of SC channel to the RIXS spectra, corresponding to Eqs. (19) and (22), respectively. Two-magnon density of states (DOS) for the extended Heisenberg antiferromagnet for (c) $J_2 = -0.1J_1$, (d) $J_2 = 0$, and (e) $J_2 = 0.1J_1$. First-order correction of spectra for (f) $J_2 = -0.1J_1$, (g) $J_2 = 0$, and (h) $J_2 = 0.1J_1$. Second-order correction of RIXS spectra for (i) $J_2 = -0.1J_1$, (j) $J_2 = 0$, and (k) $J_2 = 0.1J_1$. (l) Consolidated intensity for the SC channel that contains the total contribution to the SC channel from first and second orders in the ultrashort core-hole lifetime (UCL) expansion evaluated for $\Gamma = 5J_1$. The colormaps are generated using the same scheme as discussed in Fig. 2. The boundary value U_0 is indicated in black in the respective color bars.

where $f_0(\mathbf{k}, \mathbf{q}) = (J^{AA}_{\mathbf{k}+\mathbf{q}/2} + J^{AA}_{\mathbf{k}-\mathbf{q}/2} + J^{AA}_0 + J^{AA}_{\mathbf{q}} + J^{AB}_0 + J^{AB}_{\mathbf{q}})$ and $f_1(\mathbf{k}, \mathbf{q}) = (J^{AB}_{\mathbf{k}+\mathbf{q}/2} + J^{AB}_{\mathbf{k}-\mathbf{q}/2})$.

The first-order scattering operator in UCL approximation within the LSWT can be mapped to the two-magnon, as discussed above.

Figures 4(f)–4(h) show the response for the first-order correction in this channel. A number of striking features can be observed. The spectral weight vanishes at $\mathbf{q} = (0, 0)$ and (π, π), which follows from Eq. (20). More intuitively, since $[H_0, O_{\mathbf{q}=(0,0)}] = 0$, they have the same eigenbasis, and hence, the matrix element $\langle f|O_{\mathbf{q}=(0,0)}|g\rangle$ is zero. Thus, the intensity vanishes at the zero transferred momentum, in agreement with the experimental observation [46]. Because of the AFM ground state, the RIXS intensity always vanishes at $\mathbf{q} = (\pi, \pi)$. The $\mathbf{q} = (\pi, \pi)$ is the reciprocal magnetic lattice vector for AFM order. Setting $\mathbf{q} = (\pi, \pi)$ in Eq. (19), we find that $O_{\mathbf{q}=(\pi,\pi)} = \sum_{i\in A,j} \mathbf{S}_i \cdot \mathbf{S}_j - \sum_{i\in B,j} S_i \cdot S_j$, where A and B are two sublattice indexes. The initial state $|g\rangle$ (ground state) is symmetric under the interchange of the sublattice, whereas $O_{\mathbf{q}=(\pi,\pi)}$ is antisymmetric under the interchange of the sublattice. Therefore, $\langle f|\, O_{\mathbf{q}=(\pi,\pi)}\, |g\rangle$ vanished identically. We also notice an overall hardening in both two-magnon DOSs as well as spectral weight for negative J_2 and softening for positive J_2.

2. Second order

The second-order correction in the UCL expansion of $O(J^4/\Gamma^6)$ is given by

$$O^{\mathrm{SC}}_{\mathbf{q},2} = \sum_{i,j,k} \exp(i\mathbf{q} \cdot \mathbf{r}_i) J_{i,j} J_{i,k} (\mathbf{S}_i \cdot \mathbf{S}_j)(\mathbf{S}_i \cdot \mathbf{S}_k). \tag{22}$$

Simplifying $J_{i,j}J_{i,k}(\mathbf{S}_i \cdot \mathbf{S}_j)(\mathbf{S}_i \cdot \mathbf{S}_k)$, like the NSC channel [see Eq. (15)], there are two terms. One is the two-magnon term $(\mathbf{S}_i.\mathbf{S}_j)$ with a different prefactor, and a second term is $\frac{1}{4}J_{i,j}J_{i,k}(\mathbf{S}_j \cdot \mathbf{S}_k)$. As in the NSC channel, the first term does not contribute to any new feature. The summations over the

j, k indices in the second term are shown in Fig. 4(b). Following the approach discussed above, this term can be expressed as

$$O^{\mathrm{SC}}_{\mathbf{q},2'} \approx 2S \sum_{\mathbf{k}} f(\mathbf{k},\mathbf{q})(u_{\mathbf{k}} v_{\mathbf{k}+\mathbf{q}} + u_{\mathbf{k}+\mathbf{q}} v_{\mathbf{k}})\alpha^{\dagger}_{\mathbf{k}} \beta^{\dagger}_{-\mathbf{k}-\mathbf{q}}, \quad (23)$$

where $f(\mathbf{k},\mathbf{q}) = (J_1)^2[-6\{\cos(q_x)+\cos(q_y)\} + 2\{\cos(2k_x + q_x) + \cos(2k_y + q_y)\} + 4\{\cos(k_y)\cos(k_x + q_x) + \cos(k_x)\cos(k_y + q_y)\}]$.

Figures 4(i)–4(k) show the spectra for this response function for $J_2 = -0.1J_1, J_1$, and $0.1J_1$, respectively. For $J_2 = 0$ shown in panel (j), we notice dispersive features exist over the energy window allowed by the two-magnon DOS. However, unlike at the previous order contribution to the SC channel, we now observe clear weight at $\mathbf{q} = (0,0)$ spread between $\omega/J_1 = 3$ and 4. This weight, however, is limited between $\mathbf{q} = (0,0)$ and $(\sim\pi/2, 0)$. The other feature in the middle of the plot resembles the two-magnon features in the first-order correction. Thus, the main correction to the two-magnon spectra coming from the second order are new spectral weights around $\mathbf{q} = (0,0)$. The two-magnon term discussed above commutes with H_0 at both the first and second orders of the SC channel at $\mathbf{q} = (0,0)$. However, the term $\frac{1}{4}J_{i,j}J_{i,k}(\mathbf{S}_j \cdot \mathbf{S}_k)$ does not commute with H_0 at $\mathbf{q} = 0$ and gives rise to a finite spectral weight at the second order. The same features carry over to the cases with $J_2 = \pm 0.1J_1$, with $J_2 > 0$ ($J_2 < 0$), making the features much more dominant (suppressed), as is expected.

We conclude the discussion on the SC channel by presenting in Fig. 4(l) the consolidated contributions from the SC channel containing the first- and second-order contributions to the RIXS intensity. Unlike the NSC channel, the zeroth order does not contribute to spin excitations. As for the NSC channel, we set J_1/Γ to 5. We observe that the $q = (0,0)$ second-order feature is highly suppressed.

IV. CONCLUSIONS

We have provided a comprehensive study of the RIXS cross-section for a 2D AFM in both the NSC and SC channels up to the second-order corrections in the UCL expansion of the KH formalism relevant for the Cu L edge of 2D cuprates. We explore these corrections using LSWT. We report the observation of three-magnon excitations in the NSC channel. We find that the three-magnon has finite weights in both the first- and second-order corrections in the NSC channels, albeit the weights are larger in the second-order correction. These three-magnon excitations have a clear high-energy feature with a quasiflat band extending over the entire Brillouin zone, very distinct from the two-magnons reported in the literature. We further report that the LSWT results of the NSC channel agree qualitatively with the ED results on a small cluster.

The Cu L-edge RIXS in 2D cuprates has a large contribution from the NSC channel. We, therefore, compare our results with the Cu L_3-edge RIXS data of La_2CuO_4 reported in Ref. [31]. It shows a peculiar excitation at around $\omega =$ 350 meV, which weakly disperses in energy over the Brillouin zone center and extends up to $\mathbf{q} = (0,0)$, in addition to the one-magnon and two-magnon. Using $J_1 \approx 150$ meV, we find that the spread of the RIXS spectra qualitatively agrees with the RIXS experiment, and this feature can, therefore, be interpreted as a three-magnon. Nevertheless, our calculations restricted to the LSWT predict higher energy for the observed three-magnon than the RIXS data. This is not unexpected as three-magnons are expected to soften these excitations with the inclusion of magnon-magnon interaction in comparison with other excitations. Reference [47] reported a large softening for a three-magnon in the dynamical spin structure factor, but such an analysis for a RIXS cross-section is beyond the scope of this paper.

We further report the SC channel of the RIXS and extend the correlation functions with a long-range interaction relevant for the Cu L edge in cuprates. We find that the longer-range interaction in this channel does not qualitatively alter the features of the first- and second-order corrections. This suggests that the higher-order corrections of the NSC channel are critical to reproduce the magnetic excitations in the new phase space observed at the L edge with improved resolution of RIXS.

Thus, our result is an important step in identifying the nature of multimagnon excitations observed in the RIXS spectra of 2D AFMs [31]. We note that LSWT can be used to study both indirect and direct RIXS, although our focus here was on direct RIXS for the Cu L edge in cuprates. For example, it is understood that the SC channel is equivalent to indirect RIXS [25]. The relevance of higher-order correction in the RIXS cross-section in the 2D AFMs opens up pathways to explore the higher modes of magnetic excitations in quantum materials using RIXS. Importantly, these excitations persist at small momentum transfer, therefore, opening up pathways for exploring quantum magnets where large momentum transfer is inaccessible.

ACKNOWLEDGMENTS

All computations were performed in the NOETHER, VIRGO, and KALINGA high-performance clusters at NISER. A.M. would like to acknowledge the MATRICS grant (Grant No. MTR/2022/000636) from the Science and Engineering Research Board for funding.

APPENDIX A: UCL EXPANSION FOR KH FORMALISM

Here, we provide the relevant expressions for the NSC and SC scattering cross-sections. We refer the reader to recent literature for details [19,20]. At the L edge, the dipole operator can allow for single spin-flip excitations, leading to the following NSC contributions to the RIXS cross-section at various orders of the inverse core-hole lifetime parameter (Γ):

$$I^{\mathrm{NSC}}(\mathbf{q},\omega) \propto \left[\frac{1}{\Gamma^2}\sum_f \left|\langle f|\frac{1}{\sqrt{N}}\sum_i \exp(i\mathbf{q}\cdot\mathbf{R}_i)S^x_i|g\rangle\right|^2 + \frac{1}{\Gamma^4}\sum_f \left|\langle f|\frac{1}{\sqrt{N}}\sum_{i,j}\exp(i\mathbf{q}\cdot\mathbf{R}_i)J_{i,j}S^x_i\left(\hat{S}_i\cdot\hat{S}_j\right)|g\rangle\right|^2\right.$$

$$+\frac{1}{\Gamma^6}\sum_f\left|\langle f|\frac{1}{\sqrt{N}}\sum_{i,j,k}\exp(i\mathbf{q}\cdot\mathbf{R}_i)J_{i,j}J_{i,k}S_i^x(\hat{S}_i\cdot\hat{S}_j)(\hat{S}_i\cdot\hat{S}_k)|g\rangle\right|^2+\cdots\Big]\delta(E_f-E_g-\omega)$$
$$=\sum_l S_l^{\mathrm{NSC}}(\mathbf{q},\omega). \tag{A1}$$

In the above, the $O[(1/\Gamma)^2]$ term is the single spin-flip spin+-excitation scattering, and the $O[(1/\Gamma)^4]$ term is a combination single spin flip at the site where the core-hole is created and a bimagnon lives at either the j or k site NN to i, or a bimagnon involves i and j or i and k, as discussed in the paper.

For the SC channel, the contributions to the RIXS intensity are given by

$$I^{\mathrm{SC}}(\mathbf{q},\omega)\propto\Big[\frac{1}{\Gamma^2}\sum_f\left|\langle f|\frac{1}{\sqrt{N}}\sum_i\exp(i\mathbf{q}\cdot\mathbf{R}_i)n_{i,\sigma}|g\rangle\right|^2+\frac{1}{\Gamma^4}\sum_f\left|\langle f|\frac{1}{\sqrt{N}}\sum_{i,j}\exp(i\mathbf{q}\cdot\mathbf{R}_i)J_{i,j}\hat{S}_i\cdot\hat{S}_j|g\rangle\right|^2$$
$$+\frac{1}{\Gamma^6}\sum_f\left|\langle f|\frac{1}{\sqrt{N}}\sum_{i,j,k}\exp(i\mathbf{q}\cdot\mathbf{R}_i)J_{i,j}J_{i,k}(\hat{S}_i\cdot\hat{S}_j)(\hat{S}_i\cdot\hat{S}_k)|g\rangle\right|^2+\cdots\Big]\delta(E_f-E_g-\omega)$$
$$=\sum_l S_l^{\mathrm{SC}}(\mathbf{q},\omega). \tag{A2}$$

We note that the $O[(1/\Gamma)^2]$ term does not contribute to spin excitations. The higher-order terms lead to magnetic excitations. The bimagnon excitations from these higher orders are calculated and discussed in the paper.

APPENDIX B: CALCULATION DETAILS

The detailed expressions for $f_0(\mathbf{k},\mathbf{p},\mathbf{q})$ and $f_1(\mathbf{k},\mathbf{p},\mathbf{q})$ used in Eq. (13) in the paper are provided below, with $J^{NNN}_{\mathbf{k},\mathbf{p},\mathbf{q}}=J^{AA}_{\mathbf{k}+\mathbf{p}+\mathbf{q}}+J^{AA}_{\mathbf{k}}-J^{AA}_{0}-J^{AA}_{\mathbf{p}+\mathbf{q}}$:

$$f_0(\mathbf{k},\mathbf{p},\mathbf{q})=-\Big\{\Big[\big(J^{AB}_{\mathbf{p}+\mathbf{q}}+J^{NNN}_{\mathbf{k},\mathbf{p},\mathbf{q}}\big)u_{\mathbf{p}}-\big(J^{AB}_{0}+J^{NNN}_{\mathbf{k},\mathbf{p},\mathbf{q}}\big)v_{\mathbf{p}}\Big]u_{\mathbf{k}}v_{\mathbf{k}+\mathbf{p}+\mathbf{q}}+\Big[\big(J^{AB}_{0}+J^{NNN}_{\mathbf{k},\mathbf{p},\mathbf{q}}\big)u_{\mathbf{p}}-\big(J^{AB}_{\mathbf{p}+\mathbf{q}}+J^{NNN}_{\mathbf{k},\mathbf{p},\mathbf{q}}\big)v_{\mathbf{p}}\Big]v_{\mathbf{k}}u_{\mathbf{k}+\mathbf{p}+\mathbf{q}}\Big\}$$
$$+\big(J^{AB}_{\mathbf{k}+\mathbf{p}+\mathbf{q}}u_{\mathbf{p}}-J^{AB}_{\mathbf{k}}v_{\mathbf{p}}\big)v_{\mathbf{k}+\mathbf{p}+\mathbf{q}}v_{\mathbf{k}}+\big(J^{AB}_{\mathbf{k}}u_{\mathbf{p}}-J^{AB}_{\mathbf{k}+\mathbf{p}+\mathbf{q}}v_{\mathbf{p}}\big)u_{\mathbf{k}+\mathbf{p}+\mathbf{q}}u_{\mathbf{k}}, \tag{B1}$$

$$f_1(\mathbf{k},\mathbf{p},\mathbf{q})=-\Big\{\Big[\big(J^{AB}_{0}+J^{NNN}_{\mathbf{k},\mathbf{p},\mathbf{q}}\big)u_{\mathbf{p}}-\big(J^{AB}_{\mathbf{p}+\mathbf{q}}+J^{NNN}_{\mathbf{k},\mathbf{p},\mathbf{q}}\big)v_{\mathbf{p}}\Big]u_{\mathbf{k}}v_{\mathbf{k}+\mathbf{p}+\mathbf{q}}+\Big[\big(J^{AB}_{\mathbf{p}+\mathbf{q}}+J^{NNN}_{\mathbf{k},\mathbf{p},\mathbf{q}}\big)u_{\mathbf{p}}-\big(J^{AB}_{0}+J^{NNN}_{\mathbf{k},\mathbf{p},\mathbf{q}}\big)v_{\mathbf{p}}\Big]v_{\mathbf{k}}u_{\mathbf{k}+\mathbf{p}+\mathbf{q}}\Big\}$$
$$+\big(J^{AB}_{\mathbf{k}}u_{\mathbf{p}}-J^{AB}_{\mathbf{k}+\mathbf{p}+\mathbf{q}}v_{\mathbf{p}}\big)v_{\mathbf{k}+\mathbf{p}+\mathbf{q}}v_{\mathbf{k}}+\big(J^{AB}_{\mathbf{k}+\mathbf{p}+\mathbf{q}}u_{\mathbf{p}}-J^{AB}_{\mathbf{k}}v_{\mathbf{p}}\big)u_{\mathbf{k}+\mathbf{p}+\mathbf{q}}u_{\mathbf{k}}. \tag{B2}$$

[1] E. Dagotto, Rev. Mod. Phys. **66**, 763 (1994).
[2] D. J. Scalapino, Phys. Rep. **250**, 329 (1995).
[3] D. Li, K. Lee, B. Y. Wang, M. Osada, S. Crossley, H. R. Lee, Y. Cui, Y. Hikita, and H. Y. Hwang, Nature (London) **572**, 624 (2019).
[4] J. Bertinshaw, Y. K. Kim, G. Khaliullin, and B. J. Kim, Annu. Rev. Condens. Matter Phys. **10**, 315 (2019).
[5] P. W. Anderson, Science **235**, 1196 (1987).
[6] H. Lu, M. Rossi, A. Nag, M. Osada, D. F. Li, K. Lee, B. Y. Wang, M. Garcia-Fernandez, S. Agrestini, Z. X. Shen *et al.*, Science **373**, 213 (2021).
[7] J. Kim, D. Casa, M. H. Upton, T. Gog, Y.-J. Kim, J. F. Mitchell, M. van Veenendaal, M. Daghofer, J. van den Brink, G. Khaliullin *et al.*, Phys. Rev. Lett. **108**, 177003 (2012).
[8] F. Gel'mukhanov, M. Odelius, S. P. Polyutov, A. Föhlisch, and V. Kimberg, Rev. Mod. Phys. **93**, 035001 (2021).
[9] L. J. P. Ament, M. van Veenendaal, T. P. Devereaux, J. P. Hill, and J. van den Brink, Rev. Mod. Phys. **83**, 705 (2011).
[10] S. Kourtis, J. van den Brink, and M. Daghofer, Phys. Rev. B **85**, 064423 (2012).
[11] A. Nocera, U. Kumar, N. Kaushal, G. Alvarez, E. Dagotto, and S. Johnston, Sci. Rep. **8**, 11080 (2018).
[12] J. Schlappa, U. Kumar, K. J. Zhou, S. Singh, M. Mourigal, V. N. Strocov, A. Revcolevschi, L. Patthey, H. M. Rønnow, S. Johnston *et al.*, Nat. Commun. **9**, 5394 (2018).
[13] V. Bisogni, S. Kourtis, C. Monney, K. Zhou, R. Kraus, C. Sekar, V. Strocov, B. Büchner, J. van den Brink, L. Braicovich *et al.*, Phys. Rev. Lett. **112**, 147401 (2014).
[14] K. Wohlfeld, S. Nishimoto, M. W. Haverkort, and J. van den Brink, Phys. Rev. B **88**, 195138 (2013).
[15] D. Benjamin, I. Klich, and E. Demler, Phys. Rev. Lett. **112**, 247002 (2014).
[16] L. J. P. Ament, G. Ghiringhelli, M. M. Sala, L. Braicovich, and J. van den Brink, Phys. Rev. Lett. **103**, 117003 (2009).
[17] L. Braicovich, J. van den Brink, V. Bisogni, M. M. Sala, L. J. P. Ament, N. B. Brookes, G. M. De Luca, M. Salluzzo,

T. Schmitt, V. N. Strocov *et al.*, Phys. Rev. Lett. **104**, 077002 (2010).
[18] M. M. Sala, V. Bisogni, C. Aruta, G. Balestrino, H. Berger, N. B. Brookes, G. M. de Luca, D. D. Castro, M. Grioni, M. Guarise *et al.*, New J. Phys. **13**, 043026 (2011).
[19] U. Kumar, A. Nag, J. Li, H. C. Robarts, A. C. Walters, M. García-Fernández, R. Saint-Martin, A. Revcolevschi, J. Schlappa, T. Schmitt *et al.*, Phys. Rev. B **106**, L060406 (2022).
[20] C. Jia, K. Wohlfeld, Y. Wang, B. Moritz, and T. P. Devereaux, Phys. Rev. X **6**, 021020 (2016).
[21] J.-i. Igarashi and T. Nagao, Phys. Rev. B **85**, 064421 (2012).
[22] F. Forte, M. Cuoco, C. Noce, and J. van den Brink, Phys. Rev. B **83**, 245133 (2011).
[23] L. Braicovich, M. Minola, G. Dellea, M. Le Tacon, M. Moretti Sala, C. Morawe, J.-C. Peffen, R. Supruangnet, F. Yakhou, G. Ghiringhelli *et al.*, Rev. Sci. Instrum. **85**, 115104 (2014).
[24] R. Fumagalli, L. Braicovich, M. Minola, Y. Y. Peng, K. Kummer, D. Betto, M. Rossi, E. Lefrançois, C. Morawe, M. Salluzzo *et al.*, Phys. Rev. B **99**, 134517 (2019).
[25] F. Forte, L. J. P. Ament, and J. van den Brink, Phys. Rev. B **77**, 134428 (2008).
[26] U. Kumar, A. Nocera, E. Dagotto, and S. Johnston, New J. Phys. **20**, 073019 (2018).
[27] U. Kumar, A. Nocera, G. Price, K. Stiwinter, S. Johnston, and T. Datta, Phys. Rev. B **102**, 075134 (2020).
[28] G. Schmiedinghoff, L. Müller, U. Kumar, G. S. Uhrig, and B. Fauseweh, Commun. Phys. **5**, 218 (2022).
[29] U. Kumar, A. Nocera, E. Dagotto, and S. Johnston, Phys. Rev. B **99**, 205130 (2019).
[30] Y. Tseng, J. Thomas, W. Zhang, E. Paris, P. Puphal, R. Bag, G. Deng, T. C. Asmara, V. N. Strocov, S. Singh *et al.*, npj Quantum Mater. **7**, 92 (2022).
[31] H. C. Robarts, M. García-Fernández, J. Li, A. Nag, A. C. Walters, N. E. Headings, S. M. Hayden, and K.-J. Zhou, Phys. Rev. B **103**, 224427 (2021).
[32] D. Betto, R. Fumagalli, L. Martinelli, M. Rossi, R. Piombo, K. Yoshimi, D. Di Castro, E. Di Gennaro, A. Sambri, D. Bonn *et al.*, Phys. Rev. B **103**, L140409 (2021).
[33] M. Mourigal, M. Enderle, A. Klöpperpieper, J.-S. Caux, A. Stunault, and H. M. Rønnow, Nat. Phys. **9**, 435 (2013).
[34] B. Lake, D. A. Tennant, J.-S. Caux, T. Barthel, U. Schollwöck, S. E. Nagler, and C. D. Frost, Phys. Rev. Lett. **111**, 137205 (2013).
[35] S. Notbohm, P. Ribeiro, B. Lake, D. A. Tennant, K. P. Schmidt, G. S. Uhrig, C. Hess, R. Klingeler, G. Behr, B. Büchner *et al.*, Phys. Rev. Lett. **98**, 027403 (2007).
[36] M. Windt, M. Grüninger, T. Nunner, C. Knetter, K. P. Schmidt, G. S. Uhrig, T. Kopp, A. Freimuth, U. Ammerahl, B. Büchner *et al.*, Phys. Rev. Lett. **87**, 127002 (2001).
[37] B. Dalla Piazza, M. Mourigal, N. B. Christensen, G. J. Nilsen, P. Tregenna-Piggott, T. G. Perring, M. Enderle, D. F. McMorrow, D. A. Ivanov, and H. M. Rønnow, Nat. Phys. **11**, 62 (2015).
[38] C. Luo, T. Datta, and D.-X. Yao, Phys. Rev. B **89**, 165103 (2014).
[39] Y. Y. Peng, G. Dellea, M. Minola, M. Conni, A. Amorese, D. Di Castro, G. M. De Luca, K. Kummer, M. Salluzzo, X. Sun *et al.*, Nat. Phys. **13**, 1201 (2017).
[40] M. He, T. Datta, and D.-X. Yao, Phys. Rev. B **101**, 024426 (2020).
[41] L. Martinelli, D. Betto, K. Kummer, R. Arpaia, L. Braicovich, D. Di Castro, N. B. Brookes, M. Moretti Sala, and G. Ghiringhelli, Phys. Rev. X **12**, 021041 (2022).
[42] U. Kumar and S.-Z. Lin, Phys. Rev. B **103**, 064508 (2021).
[43] S. Li, A. Nocera, U. Kumar, and S. Johnston, Commun. Phys. **4**, 217 (2021).
[44] A. H. MacDonald, S. M. Girvin, and D. Yoshioka, Phys. Rev. B **37**, 9753 (1988).
[45] V. Bisogni, L. Simonelli, L. J. P. Ament, F. Forte, M. Moretti Sala, M. Minola, S. Huotari, J. van den Brink, G. Ghiringhelli, N. B. Brookes *et al.*, Phys. Rev. B **85**, 214527 (2012).
[46] J. P. Hill, G. Blumberg, Y.-J. Kim, D. S. Ellis, S. Wakimoto, R. J. Birgeneau, S. Komiya, Y. Ando, B. Liang, R. L. Greene *et al.*, Phys. Rev. Lett. **100**, 097001 (2008).
[47] M. Powalski, K. P. Schmidt, and G. S. Uhrig, SciPost Phys. **4**, 001 (2018).